

Article

On the Optical Properties of $\text{Cr}_2\text{Ge}_2\text{Te}_6$ and Its Heterostructure

Hiroshi Idzuchi^{1,2,3,4,*}, Andres E. Llacsahuanga Allcca⁴, Amanda Victo Haglund⁵, Xing-Chen Pan², Takuya Matsuda¹, Katsumi Tanigaki^{2,5}, David Mandrus^{6,7}  and Yong P. Chen^{2,3,4,8,9,10}

¹ Department of Physics, The University of Tokyo, Tokyo 113-0033, Japan; takuya.matsuda@phys.s.u-tokyo.ac.jp

² WPI Advanced Institute for Materials Research (AIMR), Tohoku University, Sendai 980-8577, Japan; xingchen.pan.a2@tohoku.ac.jp (X.-C.P.); katsumitanigaki@baqis.ac.cn (K.T.)

³ Center for Science and Innovation in Spintronics (CSIS), Tohoku University, Sendai 980-8577, Japan

⁴ Department of Physics and Astronomy, Purdue University, West Lafayette, IN 47907, USA; aallcca@purdue.edu

⁵ Beijing Academy of Quantum Information and Sciences, Beijing 100193, China

⁶ Department of Materials Science and Engineering, University of Tennessee, Knoxville, TN 37996, USA

⁷ Materials Science and Technology Division, Oak Ridge National Laboratory, Oak Ridge, TN 37831, USA

⁸ School of Electrical and Computer Engineering and Birck Nanotechnology Center, Purdue University, West Lafayette, IN 47907, USA

⁹ Purdue Quantum Science and Engineering Institute, Purdue University, West Lafayette, IN 47907, USA

¹⁰ Institute of Physics and Astronomy and Villum Centers for Dirac Materials and for Hybrid Quantum Materials and Devices, Aarhus University, 8000 Aarhus C, Denmark

* Correspondence: idzuchi@g.ecc.u-tokyo.ac.jp

Abstract: Recently, there has been a growing interest in two-dimensional van der Waals (vdW) magnets owing to their unique two-dimensional magnetic phenomena and potential applications. Most vdW ferromagnets have the Curie temperature below room temperature, highlighting the need to explore how to enhance their magnetism. In our previous report, we successfully increased the Curie temperature of the prototypical vdW magnet $\text{Cr}_2\text{Ge}_2\text{Te}_6$ using a NiO overlayer. In layered materials, the presence of wrinkles is often observed and evaluating them using optical microscopy proves to be useful; however, there have been limited investigations into the optical constants of vdW magnets, hampering progress in understanding their optical properties. In this study, we present the optical constants of $\text{Cr}_2\text{Ge}_2\text{Te}_6$ obtained through ellipsometry measurements. To account for the presence of wrinkles, we model a vacuum region between the substrate and the vdW magnet, and we calculate the reflectivity as a function of wavelength and vacuum thickness to visualize the optical image. Furthermore, we discuss the relationship between the optical constants and the electronic structure of the material.

Keywords: two-dimensional material; optical property; optical constant; heterostructure; multilayer



Citation: Idzuchi, H.; Llacsahuanga Allcca, A.E.; Haglund, A.V.; Pan, X.-C.; Matsuda, T.; Tanigaki, K.; Mandrus, D.; Chen, Y.P. On the Optical Properties of $\text{Cr}_2\text{Ge}_2\text{Te}_6$ and Its Heterostructure. *Condens. Matter* **2023**, *8*, 59. <https://doi.org/10.3390/condmat8030059>

Academic Editors: Ali Gencer, Annette Bussmann-Holder, J. Javier Campo Ruiz and Valerii Vinokur

Received: 30 April 2023

Revised: 3 July 2023

Accepted: 11 July 2023

Published: 14 July 2023



Copyright: © 2023 by the authors. Licensee MDPI, Basel, Switzerland. This article is an open access article distributed under the terms and conditions of the Creative Commons Attribution (CC BY) license (<https://creativecommons.org/licenses/by/4.0/>).

1. Introduction

Since the discovery of graphene, two-dimensional (2D) van der Waals (vdW) materials have attracted a lot of attention [1,2]. The isolation of graphene as a single-crystal sample with an atomically thin limit was made possible by the weak interaction between 2D layers, which is now applicable to many 2D vdW materials possessing magnetism [3,4]. Typical examples of such materials are ferromagnetic insulators $\text{Cr}_2\text{Ge}_2\text{Te}_6$ [5] and CrI_3 [6], ferromagnetic conductor Fe-Ge-Te [7], antiferromagnetic insulators FePS_3 [8], MnPS_3 [9], and $\alpha\text{-RuCl}_3$ where the last one also exhibits nontrivial spin state and has been intensively studied in the context of quantum spin liquid [3].

Two-dimensional vdW ferromagnetic insulators offer several advantages, such as the ability to obtain atomically thin crystals easily and transfer them onto flexible substrates [5,10]. $\text{Cr}_2\text{Ge}_2\text{Te}_6$ is a prototypical ferromagnet with a Curie temperature of ~60 K [3–5]. In general, 2D ferromagnets have relatively lower Curie temperature compared

to three-dimensional counterparts such as iron, cobalt, and nickel. Hence, it is crucial to increase the Curie temperature as much as possible for practical applications. Previous attempts to modify the magnetism using electrostatic gating with an electrolyte yielded limited results in terms of increasing the Curie temperature [11]. A pressure cell experiment showed that the Curie temperature decreases instead of increasing [12].

In our previous work, we reported a significant increase in the Curie temperature of the Cr₂Ge₂Te₆/NiO heterostructure, reaching ~120 K [13]. At the international conference on quantum material and technologies (ICQMT2022), we also suggested that this increase in the Curie temperature is related to the presence of wrinkle structure detected by optical microscopy, and recently we have reported that wrinkle structure and enhanced magnetism are highly correlated [14]. However, despite these advancements, the optical characterization of this material remains limited and our understanding of its optical properties is still lacking. In this paper, we investigate the optical properties of Cr₂Ge₂Te₆ and the relation to the wrinkle structure in Cr₂Ge₂Te₆/NiO. To understand the optical properties of the wrinkle structure in Cr₂Ge₂Te₆/NiO, we perform calculations on multiple reflections with numerous interfaces, which provide valuable insights into 2D materials. The optical constants of Cr₂Ge₂Te₆ are measured using ellipsometry. While optical spectroscopy has been employed to elucidate the electronic structures as well as magnetic properties, to the best of our knowledge, there have been no experimental reports on the optical constants of Cr₂Ge₂Te₆. Finally, we demonstrate that the characteristic features of the wrinkle structure in the Cr₂Ge₂Te₆/NiO can be explained based on these optical properties.

2. Results

First, we present a description of optical properties in multilayers to comprehend the optical microscope image of Cr₂Ge₂Te₆/NiO on a silicon substrate. In our previous report, we revealed that wrinkle structure appears after forming the NiO layer on Cr₂Ge₂Te₆. We anticipate that the structure includes an empty area between Cr₂Ge₂Te₆ and SiO₂/Si. Hence, we describe wavelength-dependent reflection properties up to five layers (NiO/Cr₂Ge₂Te₆/vacuum/SiO₂/Si).

2.1. Multiple Reflections on a Few-Layer Structure

2.1.1. Three Layers (Two Interfaces)

The reflection properties of the three-layer systems can be found in textbooks [15]. We employ Fresnel theory to comprehend the contrast of atomically thin flakes through multiple reflections. Let us consider three materials 0, 1, and 2 with a refractive index values of n_0 , n_1 , and n_2 , respectively. The phase shift in material 1 is represented by Δ_1 (Figure 1a).

- The fraction of the amplitude of the light which is reflected and transmitted at the interface between the material 0 and 1 are given by r_1 and $\sqrt{1 - r_1^2}$, respectively, where $r_1 = (n_0 - n_1)/(n_0 + n_1)$. Similarly, the reflection and transmission at the interface between the material 1 and 2 can be calculated. Notably, when light is penetrates from material 1 to 0, the additional phase factor, $\exp[-i\Delta_1]$ appears (Figure 1b), where $\Delta_1 = 4\pi n_1 d_1/\lambda$ and d_1 is the thickness of layer 1.

Now, we obtain the reflection R as

- $$r e^{i\epsilon}$$

$$\equiv r_1 + r_2(1 - r_1^2) \exp[-i\Delta_1] - r_1 r_2^2(1 - r_1^2) \exp[-2i\Delta_1] + \dots$$

$$= r_1 + \frac{r_2(1 - r_1^2) \exp[-i\Delta_1]}{1 + r_1 r_2 \exp[-i\Delta_1]} = \frac{r_1 + r_2 \exp[-i\Delta_1]}{1 + r_1 r_2 \exp[-i\Delta_1]}$$
- $R = |r e^{i\epsilon}|^2.$

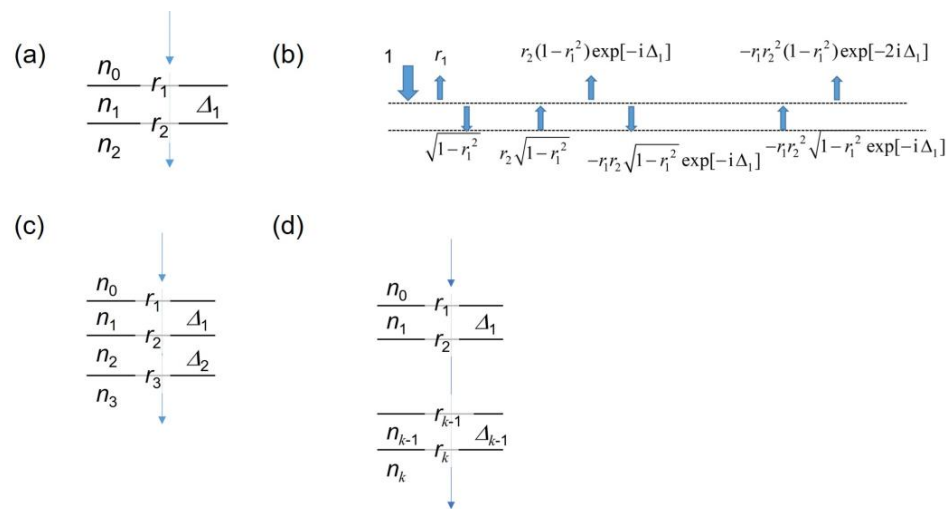


Figure 1. (a) Notation of the three layers. (b) Reflection and penetration of the light in the multilayer. The fraction of the light in each path is shown. (c) Notation of the three interfaces. (d) Notation of the general case.

2.1.2. Three Interfaces

- In a system with three interfaces (four layers), we can compare the result with the prototypical scenario of the cleaving experiment of graphene [16]. We employed Fresnel theory to understand the contrast of an atomically thin flake through multiple reflections.
- Let us consider three materials denoted as 1, 2, and 3 with refractive indices of n_1 , n_2 , and n_3 , respectively. On top of material 1, we assume the presence of air (vacuum) where the index is n_0 . The reflection of interfaces 0–1, 1–2, and 2–3 is represented by r_1 , r_2 , and r_3 , respectively. The phase shifts in materials 1 and 2 are represented by Δ_1 and Δ_2 , respectively. The schematic configuration is depicted in Figure 1c. Next, we can determine the following values: $r_2 = (n_1 - n_2)/(n_1 + n_2)$, $r_3 = (n_2 - n_3)/(n_2 + n_3)$, $\Delta_2 = 4\pi n_2 d_2/\lambda$, where λ represents the wavelength of light. The total reflection can be expressed as $R = |r^{(2)} \exp [i\epsilon(2)]|^2$ where
- $r' e^{i\epsilon'} = \frac{r_2 + r_3 \exp[-i\Delta_2]}{1 + r_2 r_3 \exp[-i\Delta_2]}$.
- $r^{(2)} e^{i\epsilon(2)} = \frac{r_1 + r' e^{i\epsilon'} \exp[-i\Delta_1]}{1 + r' r_1 e^{i\epsilon'} \exp[-i\Delta_1]}$.

The wavelength-dependent contrast is expressed as $(R [n_1 = 1] - R [n_1 = n_{\text{flake}}])/R [n_1 = 1]$. Now, let us describe the prototypical case of a graphene flake cleaved onto a silicon substrate. Figure S1 illustrates the calculated contrast of graphene on a Si substrate with a SiO₂ layer (with a thickness of 285 nm). The observation of the flake is further influenced by the sensitivity of human eyes (when a microscope is viewed through) or a camera. The sensitivity of the human eye is the highest around ~555 nm, which corresponds to the green region of the visible light spectrum [17]. The information can help determine the thickness of the SiO₂ layer to facilitate the identification of very thin flakes. If a charge-coupled device camera is used, the model has specific sensitivity, which will impact the response of the red, green, and blue channels. However, there are a number of models available that can be used with a sensitivity similar to that of human eyes. The result is consistent with the literature [16].

2.1.3. General Case

- We can generalize the calculation of the contrast for multiple layers as follows.
- The materials 1, 2, . . . , k with refractive indices of n_1, n_2, \dots, n_k , respectively. On top of material 1, we assume the presence of air (vacuum) with an index denoted as n_0 . The reflection of the interfaces 0–1, 1–2, . . . , $(k - 1) - k$ is represented by r_1, r_2 , and r_k ,

respectively. The phase shifts in material 1, 2, . . . , $k - 1$ are represented by $\Delta_1, \Delta_2, \dots, \Delta_{k-1}$, respectively. The schematic configuration is shown in Figure 1d. We can determine the following values: $r_j = (n_{j-1} - n_j)/(n_{j-1} + n_j)$, $\Delta_j = 4\pi n_j d_j/\lambda$. The total reflection can be represented as $R_k = |\tilde{r}_{c_{k-1,k}}|^2$ where

- $\tilde{r}_{c1,k} = \frac{r_{k-1} + r_k \exp[-i\Delta_{k-1}]}{1 + r_{k-1} r_k \exp[-i\Delta_{k-1}]}$.
- $\tilde{r}_{cj,k} = \frac{r_{k-j} + \tilde{r}_{c_{j-1,k}} \exp[-i\Delta_{k-j}]}{1 + r_{k-j} \tilde{r}_{c_{j-1,k}} \exp[-i\Delta_{k-j}]}$ ($j = 2, 3, \dots, k - 1$).
- The wavelength-dependent contrast is represented as $(R_k [n_1 = 1] - R_k [n_1 = n_{\text{flake}}])/R_k [n_1 = 1]$. This formula is used to understand the experiment of $\text{Cr}_2\text{Ge}_2\text{Te}_6/\text{NiO}$ (refer to Section 3.1).

2.2. Experiment

2.2.1. Method

Ellipsometry measurements were conducted using the V-VASE ellipsometer (J.A. Woollam cooperation, Lincoln, NE, USA) at three different angles ($60^\circ, 70^\circ$, and 80°) with a wavelength range of 300–1000 nm range. A bulk $\text{Cr}_2\text{Ge}_2\text{Te}_6$ crystal measuring $1 \text{ mm} \times 1 \text{ mm}$ was mounted onto the device with its c-axis aligned perpendicular to the mounting surface. To ensure a pristine surface, the incidence surface of the crystal was exfoliated using Scotch tape. The standard focusing probe accessory was used to select a flat and shiny surface on the crystal, yielding a $100 \mu\text{m}$ diameter for the incident light beam.

$\text{Cr}_2\text{Ge}_2\text{Te}_6/\text{NiO}$ sample was prepared as follows. First, $\text{Cr}_2\text{Ge}_2\text{Te}_6$ crystals were obtained by chemical vapor transport method. The crystal was mechanically cleaved onto silicon substrate (with 285 nm thick SiO_2 layer). The NiO layer was formed by sputtering. The sample was measured by using an optical microscope and atomic force microscope. A detailed procedure can be found in our previous report [13,18].

2.2.2. Result

The dielectric constants were calculated using the WVASE software (J.A. Woollam cooperation). We employed the standard generalized oscillator model ([19]: general Lorentz oscillators) and determined that two oscillators with energies of 1.703 and 3.656 eV adequately described the optical index (Figures 2 and S2).

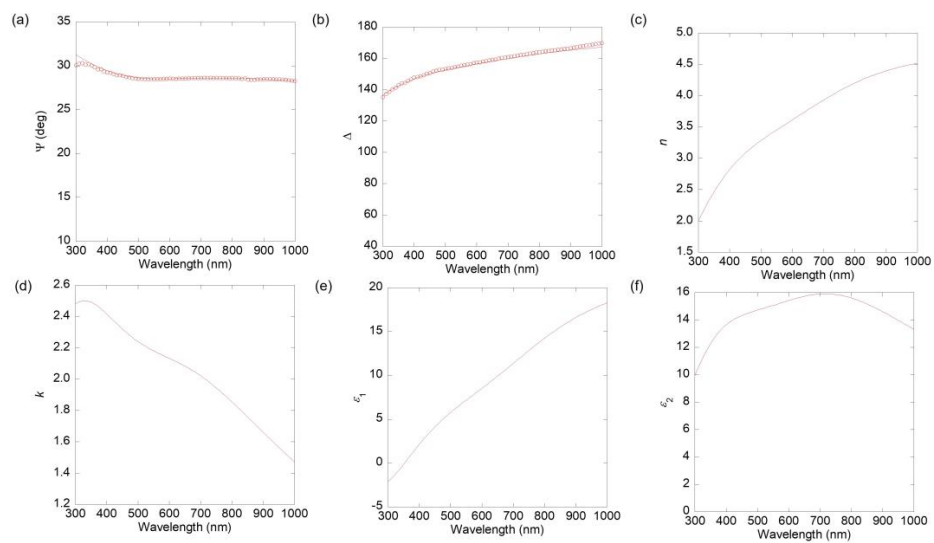


Figure 2. (a,b) Ellipsometry characterization experiment for the bulk $\text{Cr}_2\text{Ge}_2\text{Te}_6$ crystal. Wavelength dependence of Ψ (angle difference in the polarization between incident and detected light delay; see the instruction on ellipsometry [19]) and Δ (the phase difference in the polarization of incident and reflected light). (c–f) Calculated $n, k, \epsilon_1, \epsilon_2$ based on the model described in the text; n (k) represents a real (imaginary) part of the refractive index; ϵ_1 (ϵ_2) represents a real (imaginary) part of the dielectric function.

3. Discussion

3.1. Reflection Calculation on $\text{Cr}_2\text{Ge}_2\text{Te}_6/\text{NiO}$ Case

In the wrinkle structure of $\text{Si}/\text{SiO}_2/\text{Cr}_2\text{Ge}_2\text{Te}_6/\text{NiO}$, there should exist The research data generated during and/or analyzed in this manuscript are available from the corresponding author upon reasonable request. a vacuum layer between SiO_2 and $\text{Cr}_2\text{Ge}_2\text{Te}_6$. In this section, we will examine the influence of the vacuum layer on the reflection properties of this multilayer. Figure 3 shows the calculated results based on the previous section. We observed the periodicity of the reflection in $\text{Si}/\text{SiO}_2/\text{vacuum}/\text{Cr}_2\text{Ge}_2\text{Te}_6/\text{NiO}$ to be ~ 300 nm in the vacuum thickness.

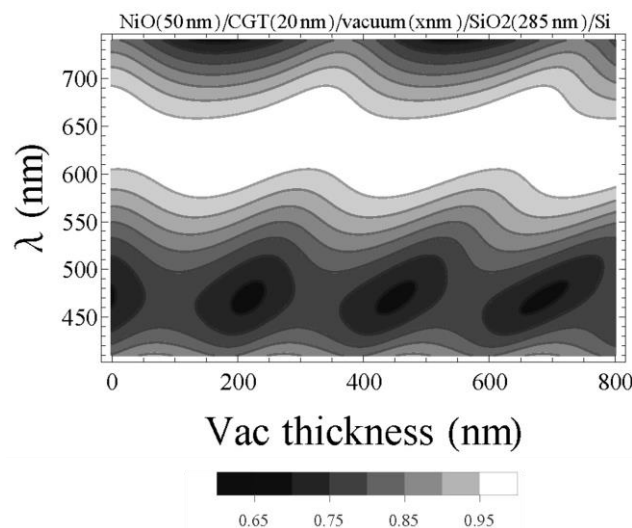


Figure 3. Calculation of the wavelength-dependent contrast $(R [n_1 = 1] - R [n_1 = n_{\text{flake}}]) / R [n_1 = 1]$ for $\text{Si}/\text{SiO}_2(285 \text{ nm})/\text{vacuum}/\text{Cr}_2\text{Ge}_2\text{Te}_6(20 \text{ nm})/\text{NiO}(50 \text{ nm})$. CGT stands for $\text{Cr}_2\text{Ge}_2\text{Te}_6$. The thickness of the vacuum layer varies from 0 nm to 800 nm.

3.2. Comparison with the $\text{Cr}_2\text{Ge}_2\text{Te}_6/\text{NiO}$ Sample

We recently reported that wrinkle structure appears, which causes enhanced magnetism. Figure 4a shows a topographic image of $\text{Si}/\text{SiO}_2/(\text{vacuum})/\text{Cr}_2\text{Ge}_2\text{Te}_6/\text{NiO}$. The wrinkle structure appears with a maximum height of $\sim 0.7 \mu\text{m}$ (Figure 4d). Figure 4b,c show the blue and red channel of the optical microscope image, which clearly shows contrast corresponding to wrinkle structure. Figure 4e shows the contrast along the wrinkle. We can observe multiple minimums in the contrast values. The period shows agreement with the reflection calculation shown in Section 3.1.

We note that the wrinkle structure is not specific to $\text{Cr}_2\text{Ge}_2\text{Te}_6/\text{NiO}$ but also appears in other 2D materials [20,21]. Our result is useful for understanding the optical contrast of these systems.

3.3. Structural and Morphological Properties

We describe the structural and morphological properties of the $\text{Cr}_2\text{Ge}_2\text{Te}_6(20 \text{ nm})/\text{NiO}(50 \text{ nm})$ heterostructure. The NiO film we used were polycrystalline; we have reported X-ray characterization on sputtered NiO films in ref. [13]; we described a transmission electron microscope image that shows polycrystallinity of the thin NiO film [14]. The surface morphology of $\text{Cr}_2\text{Ge}_2\text{Te}_6/\text{NiO}(50 \text{ nm})$ is characterized by atomic force microscopy (AFM). Figure 5 shows a representative result which shows a smooth surface with a root-mean-square (RMS) roughness of 0.23 nm. Note that the step-terrace structure of the $\text{Cr}_2\text{Ge}_2\text{Te}_6$ flake also appeared in the AFM and we chose the region of RMS excluding such a step.

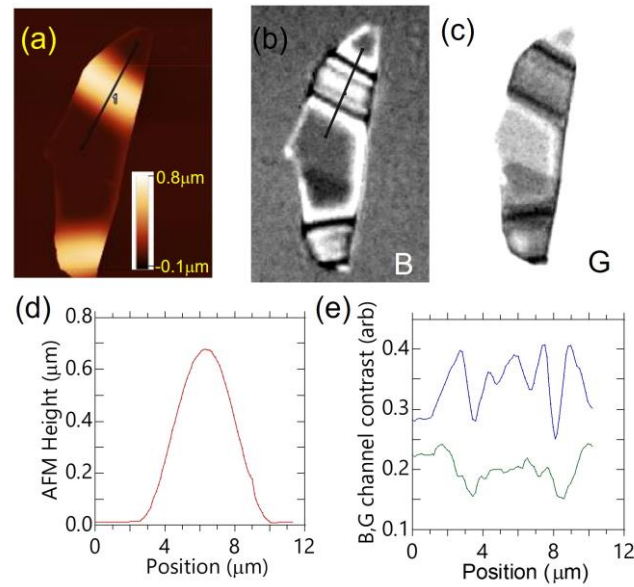


Figure 4. (a) Atomic microscope image of the $\text{Cr}_2\text{Ge}_2\text{Te}_6$ (20 nm)/NiO(50 nm) flake on Si/SiO₂(285 nm) substrate. The black line indicates the region of the data used for (d). The color bar indicates the height of the topography image. (b) The blue channel of optical contrast for the flake shown in (a). (c) The green channel of optical contrast for the flake shown in (a). (d) Line profile of height measured by AFM. The position is indicated in (a). (e) Line profile of the contrast shown in (b,c). The position is indicated in (b). The same position is used for blue and green channels.

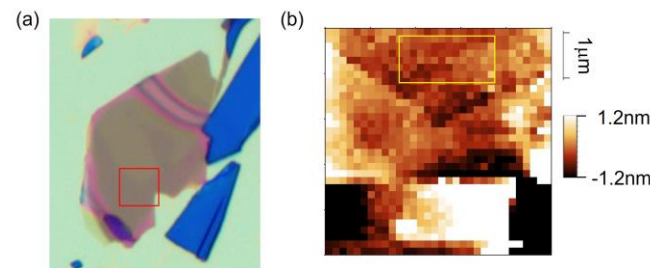


Figure 5. (a) Optical microscope image of the $\text{Cr}_2\text{Ge}_2\text{Te}_6$ flake with the NiO(50 nm) overlayer on the Si/SiO₂(285 nm). (b) AFM image for the region shown in (a) as a red rectangle. The scale bar of 1 μm in the lateral dimension and ± 1.2 nm for topography are shown. The root-mean-square roughness is 0.23 nm for the yellow rectangle region.

3.4. Comparison with Reported Density Functional

Figure 6a,b show the complex dielectric permittivity calculated by density functional theory (DFT) calculations based on ref. [22]. In Figure 6b, peaks at around 400 nm and 700 nm are shown to exist, which is in reasonable agreement with the experimental result shown in Figure 2f. However, the spectral weight in the calculation is different from in the experiment, which may be attributed to the effect of impurities or defects at the visible wavelength. Concomitantly, the screened plasma frequency in Figure 2e can be shifted towards longer wavelengths compared to the calculation in Figure 6a.

It is worth noting that the diagonal response function ϵ_{xx} obtained in this study allows for the determination of the off-diagonal response function ϵ_{xy} through the magneto-optical Kerr measurement. As $\epsilon_{xy} = (\theta_K + i\eta_K)\sqrt{\epsilon_{xx}}(1 - \epsilon_{xx})$ holds, the off-diagonal response function ϵ_{xy} rather than the Kerr rotation θ_K or the Kerr ellipticity η_K contains material information. This study therefore provides important knowledge for the magneto-optical response.

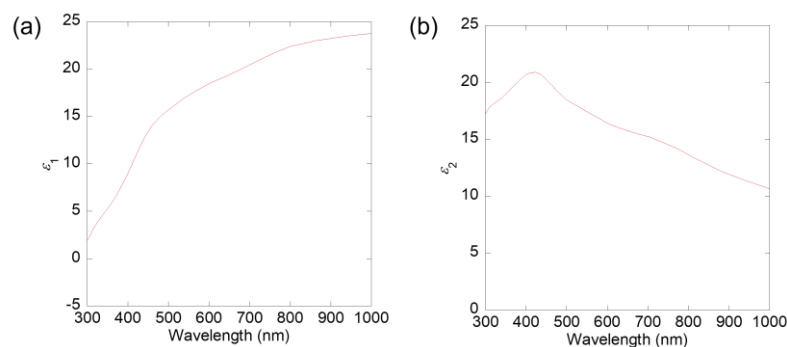


Figure 6. (a,b) Optical constant of the $\text{Cr}_2\text{Ge}_2\text{Te}_6$ bulk crystal calculated based on ref. [21].

4. Conclusions

We have studied optical properties of $\text{Cr}_2\text{Ge}_2\text{Te}_6$ and its heterostructure. We have outlined the multiple reflection on the few-layers system based on Fresnel theory. The optical index of the $\text{Cr}_2\text{Ge}_2\text{Te}_6$ crystal was characterized by ellipsometry and its implication was discussed. The optical index was used to characterize the $\text{Si}/\text{SiO}_2/\text{vacuum}/\text{Cr}_2\text{Ge}_2\text{Te}_6/\text{NiO}$ structure, and it was found to be periodic with variations in vacuum thickness. The calculation was found consistent with the contrast in the wrinkle structure of $\text{Si}/\text{SiO}_2/\text{vacuum}/\text{Cr}_2\text{Ge}_2\text{Te}_6/\text{NiO}$. The periodic contrast can be understood as not specific to the $\text{Cr}_2\text{Ge}_2\text{Te}_6/\text{NiO}$ structure but also can appear in general. This result can be used for magneto-optical research and can also be compared with the result of the wrinkle structure sometimes seen in 2D materials, which can be used as an important tuning knob [14,20] for changing physical properties.

Supplementary Materials: The following supporting information can be downloaded at: <https://www.mdpi.com/article/10.3390/condmat8030059/s1>, Figure S1: Calculation on wavelength-dependent contrast for $\text{Si}/\text{SiO}_2/\text{graphene}(\text{monolayer})$; Figure S2: Ellipsometry characterization experiment for bulk $\text{Cr}_2\text{Ge}_2\text{Te}_6$ crystal with incident angle 60, 70, and 80 deg.

Author Contributions: Conceptualization, H.I.; investigation and writing, H.I., A.E.L.A. and T.M.; investigation, A.V.H. and X.-C.P.; funding acquisition, H.I., K.T., D.M. and Y.P.C. All authors have read and agreed to the published version of the manuscript.

Funding: This work was supported in part by AIMR and its “fusion” research program in the World Premier International Research Center Initiative (WPI), Ministry of Education, Culture, Sports, Science and Technology (MEXT), Japan, by Grant-in-Aid for Scientific Research, JSPS KAKENHI (Grant Numbers, 22H01896), by the DOD MURI program (Grant Numbers, FA9550-20-1-0322), and by the Mitsubishi Foundation.

Data Availability Statement: The research data generated during and/or analyzed in this manuscript are available from the corresponding author upon reasonable request.

Conflicts of Interest: The authors declare no conflict of interest.

References

- Novoselov, K.S.; Geim, A.K.; Morozov, S.V.; Jiang, D.; Katsnelson, M.I.; Grigorieva, I.V.; Dubonos, S.V.; Firsov, A.A. Two-dimensional gas of massless Dirac fermions in graphene. *Nature* **2005**, *438*, 197. [[CrossRef](#)] [[PubMed](#)]
- Zhang, Y.; Tan, Y.W.; Stormer, H.L.; Kim, P. Experimental observation of the quantum Hall effect and Berry’s phase in graphene. *Nature* **2005**, *438*, 201. [[CrossRef](#)] [[PubMed](#)]
- Ajayan, P.; Kim, P.; Banerjee, K. Two-dimensional van der Waals materials. *Phys. Today* **2016**, *69*, 38. [[CrossRef](#)]
- Gong, C.; Zhang, X. Two-dimensional magnetic crystals and emergent heterostructure devices. *Science* **2019**, *363*, eaav4450. [[CrossRef](#)] [[PubMed](#)]
- Gong, C.; Li, L.; Li, Z.; Ji, H.; Stern, A.; Xia, Y.; Cao, T.; Bao, W.; Wang, C.; Wang, Y.; et al. Discovery of intrinsic ferromagnetism in two-dimensional van der Waals crystals. *Nature* **2017**, *546*, 265–269. [[CrossRef](#)] [[PubMed](#)]
- Huang, B.; Clark, G.; Navarro-Moratalla, E.; Klein, D.R.; Cheng, R.; Seyler, K.L.; Zhong, D.; Schmidgall, E.; McGuire, M.A.; Cobden, D.H.; et al. Layer-dependent ferromagnetism in a van der Waals crystal down to the monolayer limit. *Nature* **2017**, *546*, 270. [[CrossRef](#)] [[PubMed](#)]

7. Deng, Y.; Yu, Y.; Song, Y.; Zhang, J.; Wang, N.Z.; Sun, Z.; Yi, Y.; Wu, Y.Z.; Wu, S.; Zhu, J.; et al. Gate-tunable room-temperature ferromagnetism in two-dimensional Fe₃GeTe₂. *Nature* **2018**, *563*, 94. [CrossRef]
8. Lee, J.-U.; Lee, S.; Ryoo, J.H.; Kang, S.; Kim, T.Y.; Kim, P.; Park, C.-H.; Park, J.-G.; Cheong, H. Ising-Type Magnetic Ordering in Atomically Thin FePS₃. *Nano Lett.* **2016**, *16*, 7433–7438. [CrossRef]
9. Long, G.; Zhang, T.; Cai, X.; Hu, J.; Cho, C.; Xu, S.; Shen, J.; Wu, Z.; Han, T.; Lin, J.; et al. Isolation and Characterization of Few-Layer Manganese Thiophosphate. *ACS Nano* **2017**, *11*, 11330. [CrossRef] [PubMed]
10. Idzuchi, H.; Pientka, F.; Huang, K.-F.; Harada, K.; Gül, Ö.; Shin, Y.J.; Nguyen, L.T.; Jo, N.H.; Shindo, D.; Cava, R.J.; et al. Unconventional supercurrent phase in Ising superconductor Josephson junction with atomically thin magnetic insulator. *Nat. Commun.* **2021**, *12*, 5332. [CrossRef] [PubMed]
11. Ding, B.; Dong, B.; Li, Y.; Chen, M.; Li, X.; Huang, J.; Wang, H.; Zhao, X.; Li, Y.; Li, D.; et al. Electric-field control of magnetism in a few-layered van der Waals ferromagnetic semiconductor. *Nat. Nanotechnol.* **2018**, *13*, 554–559.
12. Sun, Y.; Xiao, R.C.; Lin, G.T.; Zhang, R.R.; Ling, L.S.; Ma, Z.W.; Luo, X.; Lu, W.J.; Sun, Y.P.; Sheng, Z.G. Effects of hydrostatic pressure on spin-lattice coupling in two-dimensional ferromagnetic Cr₂Ge₂Te₆. *Appl. Phys. Lett.* **2018**, *112*, 072409. [CrossRef]
13. Idzuchi, H.; Allcca, A.E.L.; Pan, X.C.; Tanigaki, K.; Chen, Y.P. Increased Curie temperature and enhanced perpendicular magneto anisotropy of Cr₂Ge₂Te₆/NiO heterostructures. *Appl. Phys. Lett.* **2019**, *115*, 232403. [CrossRef]
14. Idzuchi, H.; Allcca, A.E.L.; Lu, A.K.A.; Saito, M.; Houssa, M.; Meng, R.; Inoue, K.; Pan, X.-C.; Tanigaki, K.; Ikuhara, Y.; et al. Enhanced ferromagnetism in artificially stretched lattice in quasi two-dimensional Cr₂Ge₂Te₆. *arXiv* **2023**, arXiv:2306.08962v1.
15. Anders, H. *Thin Films in Optics*; Focal: London, UK, 1967; Pt. 1; pp. 47–48.
16. Blake, P.; Hill, E.W.; Neto, A.H.C.; Novoselov, K.S.; Jiang, D.; Yang, R.; Booth, T.J.; Geim, A.K. Making graphene visible. *Appl. Phys. Lett.* **2007**, *91*, 063124. [CrossRef]
17. Human Vision and Color Perception. Available online: <https://www.olympus-lifescience.com/en/microscope-resource/primer/lightandcolor/humanvisionintro/#:~:text=When%20fully%20light%20adapted%2C%20the,of%20the%20visible%20light%20spectrum> (accessed on 12 March 2023).
18. Allcca, A.E.L.; Idzuchi, H.; Pan, X.C.; Tanigaki, K.; Chen, Y.P. Modified magnetism in heterostructures of Cr₂Ge₂Te₆ and oxides. *AIP Adv.* **2023**, *13*, 015031. [CrossRef]
19. Standard Operating Procedures of Tools in Quattrone Nanofabrication Facility. Available online: https://www.seas.upenn.edu/~nanosop/documents/Session1A_UPenn_WVASE_Feb_2014.pdf (accessed on 12 March 2023).
20. Castellanos-Gomez, A.; Roldán, R.; Cappelluti, E.; Buscema, M.; Guinea, F.; van der Zant, H.S.J.; Steele, G.A. Local Strain Engineering in Atomically Thin MoS₂. *Nano Lett.* **2013**, *13*, 5361. [CrossRef] [PubMed]
21. Matuda, N.; Baba, S.; Kinbara, A. Internal stress, young's modulus and adhesion energy of carbon films on glass substrates. *Thin Solid Film.* **1981**, *81*, 301. [CrossRef]
22. Fang, Y.; Wu, S.; Zhu, Z.-Z.; Guo, G.-Y. Large magneto-optical effects and magnetic anisotropy energy in two-dimensional Cr₂Ge₂Te₆. *Phys. Rev. B* **2018**, *98*, 125416. [CrossRef]

Disclaimer/Publisher's Note: The statements, opinions and data contained in all publications are solely those of the individual author(s) and contributor(s) and not of MDPI and/or the editor(s). MDPI and/or the editor(s) disclaim responsibility for any injury to people or property resulting from any ideas, methods, instructions or products referred to in the content.